Diffusion model for austenite formation kinetics during inter-critical annealing of dual-phase steels

Patrice Chantrenne, Michel Perez, Mélanie Ollat, Véronique Massardier-Jourdan, Damien Fabrègue, Philippe Rocabois

Diffusion model for austenite formation kinetics during inter-critical annealing of dual-phase steels

P Chantrenne[1], M Perez[1], M Ollat[1], V Massardier[1], D Fabrègue[1] and P Rocabois[2]

[1] Université de Lyon—INSA Lyon—MATEIS—UMR CNRS 5510, F-69621 Villeurbanne, France
[2] Fives Keods, 108-112 Avenue de la liberté, F-94700 Maison-Alfort, France

E-mail: patrice.chantrenne@insa-lyon.fr

Abstract

A numerical solution for the ferrite-to-austenite phase transformation in a ternary iron alloy is proposed that predicts austenite formation during iso-thermal treatment. As the solution ensures perfect mass conservation of the solutes, it can be applied for long holding times until the system reaches final thermodynamic equilibrium. The solution was validated using previous experimental results on Fe–Ni–Cr alloys. Comparison with experimental data for a low-C, low-alloyed dual-phase steel enabled investigation of the effect of the initial concentration of the substitutional solute in cementite and the dis-solution of cementite on the austenite formation kinetics.

Keywords: dual phase steel, austenite formation, numerical simulation

1. Introduction

Advanced high-strength steels (AHSSs) have been widely used and developed since the mid-1970s because of their good compromise between strength and ductility, resulting in lighter and safer structures for various transport applications [1]. Dual-phase (DP) steels are some of the most widely used AHSSs; they are typically produced by thermal treatment that includes partial austenitization steps. This industrial thermal treatment consists of heating to a holding temperature (760 °C–840 °C) for 20–200 s followed by fast cooling before and after a zinc bath (460 °C). The final structure consists of ferrite and martensite to combine stamping ability with high-strength. This partial austenitization stage, or so-called intercritical

annealing, is of major importance because it controls the ferrite to austenite phase ratio and final ferrite to martensite ratio after quenching. Austenitization is therefore a footprint of the final steel microstructure, which governs the mechanical properties. However, the mechanisms of austenite formation are complex as austenite may nucleate and grow from various microstructures and because phase transformation results from the redistribution of elements with significantly different diffusivities.

In low-C, low-alloyed DP steels, austenite formation is driven first by carbide dissolution and then by carbon diffusion in austenite and ferrite. Then, austenite grows via substitutional redistribution from ferrite and finally via very slow equilibration of phases controlled by substitutional diffusion in the austenite [2, 3]. Austenite formation may also interact with the recrystallization during intercritical annealing treatment of cold-rolled steels [4–6].

Modelling the phase transformation during thermal treatments remains an issue for the proposal of new optimization routes for microstructures and thus their final properties. These coupled problems between diffusion and phase change have been investigated for many years. Solutions were first developed for heat-transfer problems [7, 8] and then adapted for mass-transfer problems. To avoid the drawbacks of conventional numerical solutions, which assume a sharp interface (the solutes are not conserved), Illingworth *et al* [9] proposed a new numerical scheme based on mathematical transformation of differential equations. However, their solution is accurate at the expense of computational cost (the time step and space step must be small). A review of numerical solutions developed for austenite-to-ferrite transformation was performed by Gouné *et al* [10]; the solutions depend on the way in which the physical phenomena leading to phase change are modelled. Austenite-to-ferrite transformation occurs during the cooling part of thermal treatment e.g. from steel that has been previously fully austenitized. Nucleation and crystal grain growth might be modelled using the Johnson–Mehl–Avrami–Kolmogorov (JMAK) model [11]. This model might also be used to predict ferrite-to-austenite transformation during the heating and holding part of thermal treatment in the intercritical domain [6, 12]. However, the JMAK model lacks a physical basis, limiting its ability to predict phase transformation for large experimental domains. Crespo *et al* [13] implemented the JMAK model using a statistical mean field approach to predict the time-dependent grain size and kinetic growth. Later, the JMAK model was modified to account for the coupling between diffusion and interface-dependent grain growth [14]. Christian [15] proposed a model for the interface growth kinetics. This approach is now widely used in the framework of the mixed mode model (accounting for the diffusion and interface-dependent propagation) either considering a sharp interface [16, 17] or a finite-sized interface [18, 19]. The interface problem has also been addressed since the 1960s with the development of phase-field methods [20]. A framework to account for the phase change induced by species diffusion was proposed by Gurtin [21] and applied to study austenite-to-ferrite transformation [22–24]. However, very few studies have focused on the ferrite-to-austenite transformation [16, 25–27].

In the intermediate stage, and typically before annealing for cold-rolled DP steel, DP steel is composed of ferrite and cementite. Commercial software such as the diffusion module of Thermo-Calc, DICTRA [28], can be used to simulate cementite dissolution and austenite formation in the three-phase (cementite, austenite, and ferrite) system and across the two interfaces (cementite/austenite and austenite/ferrite). However, Lai *et al* [2] reported that DICTRA does not predict the expected theoretical final thermodynamic equilibria because of the non-conservation of mass resulting from numerical discretization, as also reported in [29, 30].

Thus, to simulate this austenitization process, the simplified model presented in section 2 is proposed. This model considers only two phases (austenite and ferrite). To overcome the

mass conservation problem, an original numerical solution of the model is developed (section 3). The austenite fraction is then calculated for Fe–Cr–Ni alloys for comparison with previous literature results [29–31]. The model is then used to predict the austenite fraction in a DP Fe–C–Mn steel for various holding temperatures, initial concentrations of solute in cementite, and system sizes (section 4). As the proposed model only considers two phases, it is assumed that cementite instantaneously transforms into austenite. The results are compared with those obtained using DICTRA [28] simulating cementite dissolution and austenite nucleation to elucidate the effect of cementite dissolution on the austenite formation kinetics [6]. Final comparison with experimental results enables examination of the underlying physical phenomena.

2. Model

As for all models of solid phase transformation in metals, it is assumed that all the phases have the same density. The volume change is actually approximately 1% between austenite and ferrite; therefore, this assumption does not lead to significant error. This simplification is of major importance for numerical solutions because volume change has not been taken into account. The model addresses ternary systems composed of Fe, X, and Y elements. The phase transformation interface has no thickness, and the species concentrations on both sides are at thermodynamic equilibrium concentrations.

To validate the model, it is first applied to an Fe–Cr–Ni steel; therefore, X and Y are Cr and Ni, respectively. In these steels, austenite and ferrite are both present at the beginning of the isothermal treatment. Therefore, our two-phase model is well adapted. The main application of this model considers a low-alloyed C–Mn steel. Therefore, X is C and Y is Mn in the model description. Before the thermal treatment, the system is composed of cementite and ferrite. During the thermal treatment, cementite will dissolve and austenite will nucleate and grow. As the three phases cannot be addressed with the proposed model, it is assumed that cementite is instantaneously transformed into austenite, which leads to some assumptions for the initial concentration field described below.

The volume fraction of cementite (f_c), mass fractions in cementite (C_c^i), and bulk composition (C_b^i) are known for the two diffusive elements i ($i = \mathrm{C}$ or Mn). The mass fractions in ferrite (C_α^i) are then calculated using mass balance:

$$C_b^i = f_c\, C_c^i + (1 - f_c) C_\alpha^i. \tag{1}$$

To avoid accounting for cementite dissolution and austenite nucleation (leading to three phases and two interfaces), cementite is assumed to be instantaneously transformed into austenite. This assumption leads to a local carbon concentration that is higher than that of equilibrium austenite/cementite; the validity of this hypothesis will be analysed in section 4. The main drawback of this assumption is that, considering the initial C and Mn concentrations in cementite, austenite cannot be in equilibrium with ferrite at the interface. Thus, one assumes that in a small fraction δ of the original cementite near ferrite, C has diffused in ferrite to form austenite without Y diffusion. The carbon concentrations in austenite and ferrite are calculated using the tie-line with no partitioning (figure 1). From mass balance, the fraction of austenite is equal to:

$$f_\gamma = \frac{\delta C_c^C + C_\alpha^C (1 - f_c) - C_{e\alpha}^C (1 - f_c + \delta)}{C_{e\gamma}^C - C_{e\alpha}^C}. \tag{2}$$

Representations of the initial concentrations of C and Mn in the system are shown in figure 2.

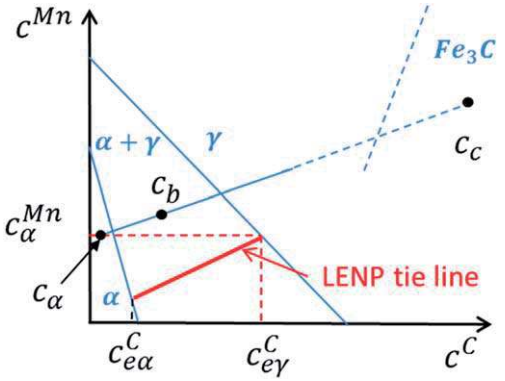

Figure 1. Schematic representation of isothermal thermodynamic equilibrium diagram of Fe–Mn–C system. Four domains are qualitatively represented: austenite (γ), ferrite (α), austenite + ferrite, and cementite. The three points represent the position of the bulk composition (C_b), cementite composition (C_c) and ferrite composition (C_α) in the initial state.

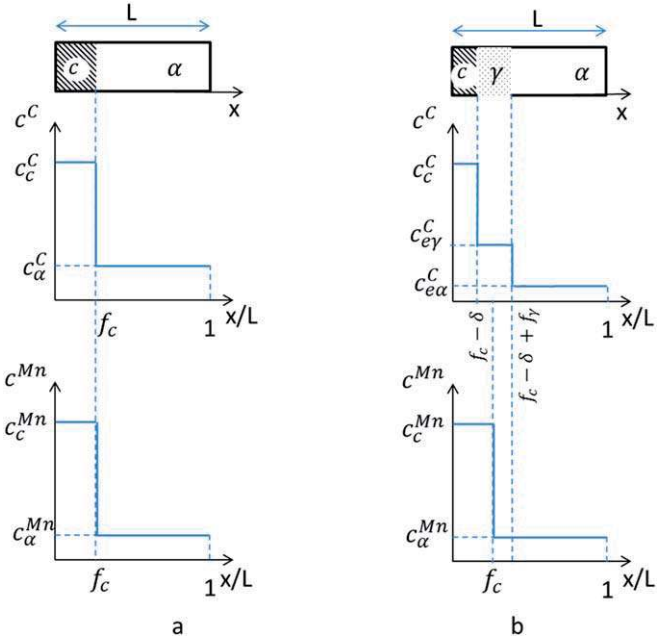

Figure 2. C and Mn concentration profiles (a) in the initial cementite–ferrite state and (b) after the selected assumption of instantaneous cementite dissolution into austenite, generating a fine layer of austenite in local equilibrium with ferrite (LENP, starting state of the model).

The goal of the model is to calculate the evolution of the austenite fraction during the isothermal holding. Therefore, the variation of the X and Y concentrations in the two phases and the position of the austenite/ferrite interface (L_γ) must be calculated.

In each phase (α for ferrite and γ for austenite) and for each species, the concentration variation during isothermal treatment is given by Fick's diffusion equations (the contribution of interdiffusion is neglected). At the sample boundaries ($x = 0$ and $x = L$, where L is the system size), the fluxes are equal to zero. Assuming that the species are at thermodynamic equilibrium at the austenite/ferrite interface, the concentrations on the austenite and ferrite sides are given by equilibrium conditions ($c^i_{e\gamma}$, $c^i_{e\alpha}$). The differential equations to be solved are

$$\frac{\partial c^i_\gamma}{\partial t} = D^i_\gamma \frac{\partial^2 c^i_\gamma}{\partial x^2}, \tag{3a}$$

with

$$\frac{\partial c^i_\gamma}{\partial x} = 0 \text{ at } x = 0 \text{ and } c^i_\gamma = c^i_{e\gamma} \text{ at } x = L_\gamma, \tag{3b}$$

$$\frac{\partial c^i_\alpha}{\partial t} = D^i_\alpha \frac{\partial^2 c^i_\alpha}{\partial x^2}, \tag{4a}$$

with

$$c^i_\alpha = c^i_{e\alpha} \text{ at } x = L_\gamma \text{ and } \frac{\partial c^i_\alpha}{\partial x} = 0 \text{ at } x = L, \tag{4b}$$

where D^i_γ and D^i_α are the diffusion coefficients of species i in austenite and ferrite, respectively. The phase change front velocity for each species, v^i, is calculated from the mass balance condition at the interface:

$$(c^i_{e\gamma} - c^i_{e\alpha})v^i = D^i_\gamma \frac{\partial c^i_\gamma}{\partial x} - D^i_\alpha \frac{\partial c^i_\alpha}{\partial x}. \tag{5}$$

As the interface velocity must be the same for the two species, this condition imposes the selection of the tie-line, which then varies as a function of time.

3. Numerical solution

3.1. Description of the solution

An analytical solution of such a system, consisting of four second-order differential equations (equations (3) and (4) for the two species) coupled with a mass conservation equation (equation (5)) by using a thermodynamic equilibrium diagram, does not exist. Numerical solutions have been developed for many years. Two types of methods have been proposed: front tracking methods [7] and homogenization methods [32]. The front tracking method based on the Murray Landis space discretization [7] (variable space grid with a constant node number in each phase) is most often used [6, 29, 30, 33]. In our solution, a constant space grid was selected for three reasons: 1—it avoids interpolations resulting from moving nodes, 2—it minimizes numerical error due to space grid variation, and 3—the space grid never tends to zero when one phase fraction becomes negligible. The geometric discretization is thus based on a constant space step Δx.

The interface position (L_γ) determines the node number in the austenite (n_γ) and ferrite (n_α) phases. An additional node with the same space step Δx is dedicated to the volume around the interface, which is allowed to move within the volume around this node (figure 3). During simulation, if the interface moves in the volume of the first node of ferrite, then one node is added to austenite and one node is subtracted from ferrite. Similarly, if the interface

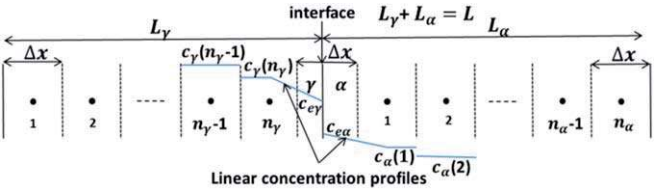

Figure 3. Principle of spatial discretization and concentration profile approximation near the austenite/ferrite interface.

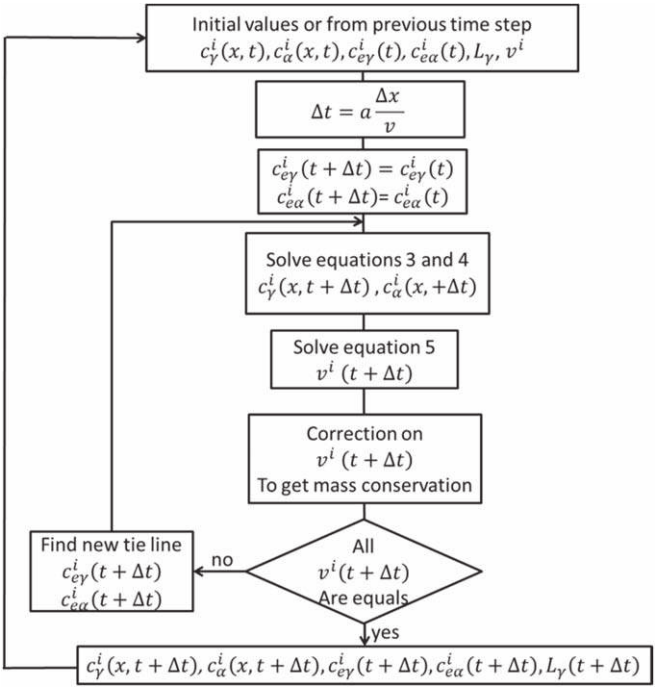

Figure 4. Algorithm for the numerical solution ensuring description of moving interface problems.

moves in the volume of the last node of austenite, then one node is subtracted from austenite and one node is added to ferrite such that the total length (L) of the system remains constant.

The time space is discretized using a time step Δt. Equations (2) and (3) are discretized using finite difference with an implicit scheme for the time derivative and a centred scheme for the second space derivative [34–36]. The algorithm used to solve the coupled equations is described in figure 4:

– At $t = 0$, the initial concentration profiles are obtained using the instantaneous cementite dissolution model described in section II (figure 2 and equation (2)). The first tie-line is determined by calculating the interface velocity of the two species using equation (4) for a large set of tie-lines to identify the tie-line for which the two interface velocities are the same.

– The time step is calculated from the interface velocity and space step to avoid too large of a displacement of the interface:

$$\Delta t = a\frac{\Delta x}{v}. \tag{6}$$

The parameter a is a numerical parameter and must be less than 1. During the simulation, the interface velocity varies by several orders of magnitude. The time step is adjusted at each time step to ensure that the interface displacement does not exceed the space step and to optimize the computational time. The parameter a is adjusted such that convergence is fulfilled at each time step.

– Equations (3) and (4) are solved to calculate the concentration gradient in the two phases. An implicit scheme is used for the time derivative to increase the stability of the numerical scheme.

– Equation (5) ensures the mass conservation and is solved to calculate the new interface velocities for each phase. As shown in figure 3, the concentration profile is assumed to be linear between the last node in austenite (the first node in ferrite) and the interface position. This assumption avoids numerical discontinuity and instabilities when the interface position changes from one node to another. However, even with the linear description of the concentration field near the interface, the approximation of the first derivative of the concentration field near the interface in equation (5) is not accurate enough and leads to non-conservation of the X and Y compounds. To improve the solution, several methods have been proposed; however, they are either computationally time consuming [9] or not accurate enough [29]. Instead of trying to find a better numerical approximation, we adjusted the interface velocities: as it appears that the mass of each species varies linearly with the interface velocity, a simple linear correction was applied to the interface velocity to determine the correct mass of each species; this solution is efficient because no iterations are necessary.

– The convergence criterion is based on the difference between the interface velocities of the two species. If the two interface velocities differ, then a new tie line should be selected using the least mean square method. This step thus requires iterations (internal loop) and a convergence parameter. Because of this loop, the selection of the tie line is implicit, which is coherent with the treatment of equations (3) and (4). If the two interface velocities are equal, then the next time step may be calculated (outer loop). For the Fe–Mn–C DP steel, the determination of the appropriate tie-line is complicated because the effect of the tie-line on the interface velocity differs greatly for the two species. This difference originates from the thermodynamic equilibrium diagram (a small variation in the C concentration has a large effect on the tie-line selection) and the difference between the C and Mn diffusion coefficients.

3.2. Comparison with previous literature results

The proposed numerical solution was first compared with that presented by Vitek *et al* [30] and Saied *et al* [29]. The case study corresponds to the ferrite–austenite transformation of a stainless-steel alloy (Fe, 30 wt% Cr, 4.5 wt% Ni). The material was initially composed of austenite and ferrite, with known fractions and compositions. Compared with the model presented in section 2, X was replaced by Cr and Y was replaced by Ni. We used the interfacial equilibrium concentrations and diffusion coefficients proposed by Saied *et al.* The austenite fraction variations during an isothermal treatment at 1100 °C are shown in figure 5.

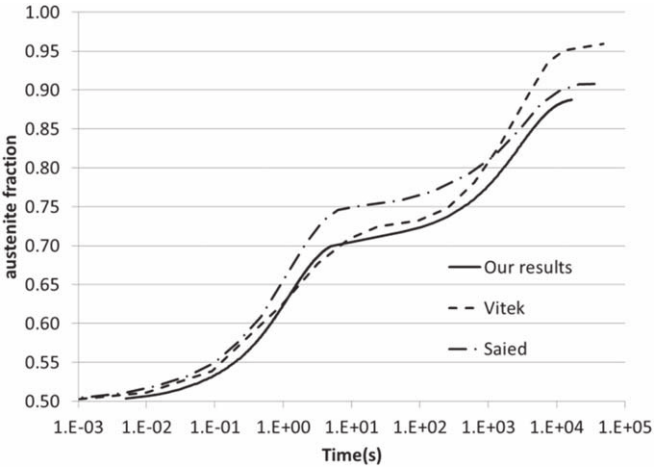

Figure 5. Comparison of the proposed model with the models presented by Vitek *et al* and Saied *et al* to predict the austenite formation kinetics in a Fe–Cr–Ni alloy during isothermal treatment at 1100 °C [29, 30].

Our model compares well with the results previously published by Vitek *et al* and Saied *et al.* However, the final equilibrium values reported by Vitek *et al* and Saied *et al* differ from the ortho-equilibrium value given in the TCFE6 database. This discrepancy originates from the non-conservation of the mass balance of their numerical solutions. This is not the case for our model because the mass balance is naturally integrated in the resolution of equation (5).

For other Fe–Cr–Ni alloys, Kajihara *et al* [31] published experimental results for the ferrite-to-austenite transformation during isothermal treatment at 1100 °C. Four different systems corresponding to four system initial sizes and compositions were considered. The same description of the equilibrium thermodynamic diagram as that used by Kajihara *et al* was used. In their paper, Kajihara *et al* also developed a numerical solution. However, they fitted the diffusion coefficients such that the numerical solutions resulted in comparable values and variations as the experimental results. To avoid this bias, we used the diffusion coefficients from [30, 37] for Cr and Ni in ferrite and austenite, respectively. As shown in figure 6, our model is in very good agreement with the experimental results without the use of any fitting parameters.

These two comparisons help validate our proposed model and its numerical solution. The solute mass is perfectly conserved, leading to the appropriate values of the final equilibrium fractions.

4. Austenite formation kinetics in a DP steel

4.1. Material and data

The model was then applied to predict the austenite formation kinetics of an industrially manufactured DP1000 steel. The steel was hot-rolled at 874 °C and then coiled at 630 °C before being naturally cooled to room temperature. It was then cold-rolled with a 55% reduction ratio to produce 1.5 mm thick steel sheets. The exact alloy composition is given in [6]. It was simplified to a ternary Fe–0.17C–1.763Mn (wt%) system with the assumption that C and Mn elements are the major elements in the austenite formation [3, 38, 39]. To

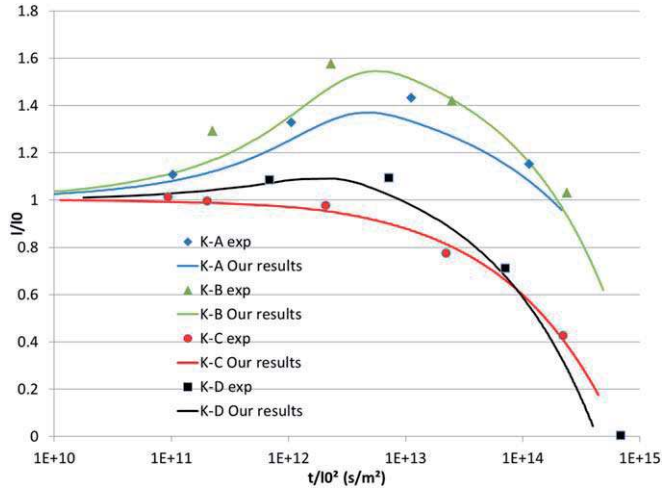

Figure 6. Evolution of experimental and modelled austenite–ferrite front position of Fe–Cr–Ni alloys during isothermal treatment at 1100 °C. The experimental values were obtained [31] for different initial ferrite lengths l_0 and different solute concentrations (given in wt%) and an initial austenite length of 2 μm (A: $l_0 = 187$ μm, 38Cr in α, 27Cr 28Ni in γ; B: $l_0 = 124$ μm, 38Cr in α, 13Cr 15Ni in γ; C: $l_0 = 130$ μm, 37Cr 28Ni in α, 24Cr 32Ni in γ; D: $l_0 = 71$ μm, 23Cr 1Ni in α, 13Cr 15Ni in γ).

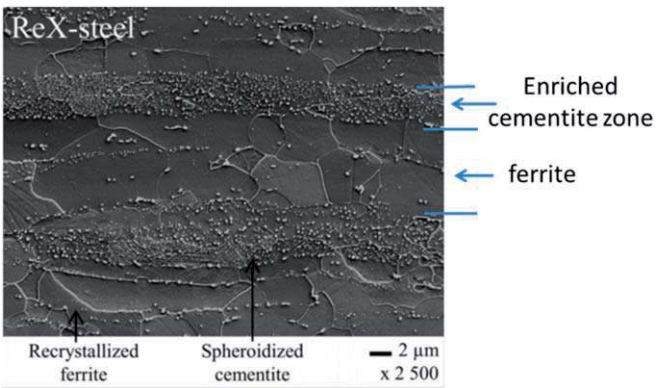

Figure 7. Optical micrograph of DP steel after recrystallization (from [6]).

decorrelate the recrystallization and phase transformation phenomena, then samples were recrystallized by a 1200 s treatment at 700 °C ($<Ac1$). The steel was initially composed of bands of recrystallized ferrite and spheroidized cementite (figure 7). The fraction of cementite was equal to $f_c = 2.44\%$. The Mn content of cementite was determined to be 13 wt% using energy-dispersive x-ray spectroscopy and carbon replica [40]. After recrystallization, the samples were heat treated using a Gleeble 3500 thermomechanical simulator. The samples were heated at 735 °C, 760 °C, and 780 °C (heating rate of 100 °C s^{-1}) and held for 1–10^6 s. After each thermal treatment, the austenite fraction was determined using metallography and image analysis. More details on the experimental protocol are given in [6].

Table 1. C and Mn diffusion coefficients in ferrite and austenite taken from MOBFE3 Thermo-Calc database for the Fe–0.17C–1.76Mn system (wt%).

	D_{α}^{C}	D_{γ}^{C}	D_{α}^{Mn}	D_{γ}^{Mn}
D_0(m s^{-2})	9.88×10^{-5}	1.73×10^{-5}	4.576	1.71×10^{-5}
Q (kJ mol^{-1})	115.830	144.214	321.869	263.183

To simulate austenite growth in this system and for comparison with experimental data, the real geometry of the microstructure shown in figure 7 was modelled. The samples consisted of layers of recrystallized ferrite (thickness = 7.5 μm) separated by layers of cementite-enriched ferrite (thickness = 2.5 μm). There are clearly two characteristic scales: the period of the layers, which approximately equals $L_p = 10$ μm, and the average distance between cementite particles in the cementite-enriched ferrite, which is much less than 1 μm. Two scenarios are considered:

- In the first one, called scenario one, the material is replaced by a layer of pure cementite (thickness of $f_c L_p$) separated by a layer of pure ferrite (thickness of $(1 - f_c)L_p$). The layer of pure cementite is assumed to immediately transform into austenite at time $t = 0$ of the simulation (see figure 2).
- In the second one, called scenario two, the cementite-enriched layer is replaced by an equivalent layer of the same thickness in which the C and Mn concentrations are equal to their average concentration. This layer is assumed to immediately transform into austenite at time $t = 0$ of the simulation.

The diffusion coefficients used for the investigated system and the temperature ranges are given in table 1. These values were extrapolated from the mobility database of Thermo-Calc (MOBFE3). To describe the tie-lines at each temperature level, the functions giving the equilibrium concentrations of C and Mn at the interface were fitted by a second-order polynomial (equation (7)). The entry parameter is the Mn equilibrium concentration of austenite ($c_{e\gamma}^{Mn}$):

$$c_e^i = a(c_{e\gamma}^{Mn})^2 + bc_{e\gamma}^{Mn} + c. \tag{7}$$

Table 2 provides the a, b, and c coefficients of these functions for the three isothermal treatment temperatures considered. The determination of these coefficients was realized by calculating the thermodynamic equilibria with TCFE5 for different Mn concentrations in austenite.

Figure 8 compares the transformation kinetics determined for scenarios one and two. It is apparent that the scenarios only differed for simulation times of less than 10 s. Considering the experimental heating rates and holding times, such short simulation times are inaccessible experimentally. Therefore, both scenarios can be considered to be equivalent. In the following, scenario one will be considered because the austenite fraction starts from 2.44% (instead of 25% for scenario two, which is unrealistic).

4.2. Comparison with Thermo-Calc diffusion module

Using scenario one, the austenite formation kinetics were predicted using our model. The results are compared with those obtained using the diffusion module of Thermo-Calc (referred to as DICTRA in the associated figures). Comparison of the austenite formation kinetics during isothermal holding at 780 °C was performed. The DICTRA calculations were

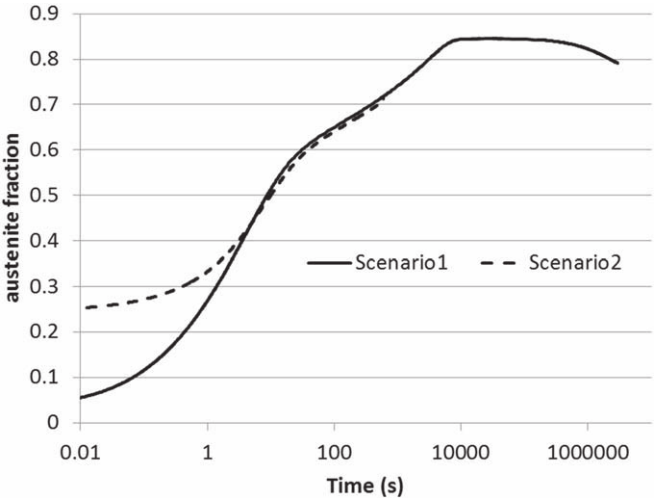

Figure 8. Comparison of evolution of austenite fraction for scenarios one and two. Simulation conditions: $L = 10\ \mu$m, $T = 780\ ^{\circ}$C, $c_c^{\mathrm{Mn}} = 13$ wt%.

Table 2. Coefficients a, b, and c of equation (7) to evaluate equilibrium concentrations c_{ei}^{X} (in wt%) of Fe–0.17C–1.76Mn system function of Mn content of austenite for temperatures of 735 °C, 760 °C, and 780 °C (extrapolated from TCFE5 Thermo-Calc database).

Evaluated equilibrium concentration c_{ei}^{X}	Coefficients a, b, and c of equation (5)	$T = 735\ ^{\circ}$C	$T = 760\ ^{\circ}$C	$T = 780\ ^{\circ}$C
$c_{e\alpha}^{\mathrm{C}}$	a	9.0609×10^{-5}	$9.457\,38 \times 10^{-5}$	$9.523\,09 \times 10^{-5}$
	b	$-3.867\,11 \times 10^{-3}$	$-4.011\,19 \times 10^{-3}$	$-4.162\,39 \times 10^{-3}$
	c	$1.822\,48 \times 10^{-2}$	$1.572\,89 \times 10^{-2}$	$1.385\,23 \times 10^{-2}$
$c_{e\gamma}^{\mathrm{C}}$	a	$-6.865\,81 \times 10^{-3}$	$-5.861\,09 \times 10^{-3}$	$-8.189\,64 \times 10^{-3}$
	b	$-9.232\,46 \times 10^{-2}$	$-9.810\,13 \times 10^{-2}$	$-9.350\,17 \times 10^{-2}$
	c	$7.000\,15 \times 10^{-1}$	$5.415\,78 \times 10^{-1}$	$4.327\,61 \times 10^{-1}$
$c_{e\alpha}^{\mathrm{Mn}}$	a	$2.987\,20 \times 10^{-2}$	$2.781\,95 \times 10^{-2}$	$2.721\,22 \times 10^{-2}$
	b	$2.411\,80 \times 10^{-1}$	$3.191\,22 \times 10^{-1}$	$3.663\,02 \times 10^{-1}$
	c	$1.363\,96 \times 10^{-2}$	$3.030\,47 \times 10^{-3}$	$1.891\,05 \times 10^{-3}$

performed using the MOBFE3 mobility database with implicit condition and varying activities. To evaluate the effect of the cementite dissolution assumption, the initial DICTRA system was set up as a two-phase cementite–ferrite problem (scenario one). Austenite was defined as an inactive phase in between cementite and ferrite to consider austenite nucleation, an option of the diffusive module. Austenite nucleates when the driving force for precipitation is greater than 10^{-5} RT. The initial C and Mn concentrations are described in figure 2(a); the C and Mn concentrations in ferrite were deduced from the mean concentrations of the alloy and the cementite fraction and initial C and Mn concentrations in cementite. The numbers of nodes in each phase were automatically adjusted in the DICTRA module and were initially set as 25 and 50, respectively, in cementite and ferrite.

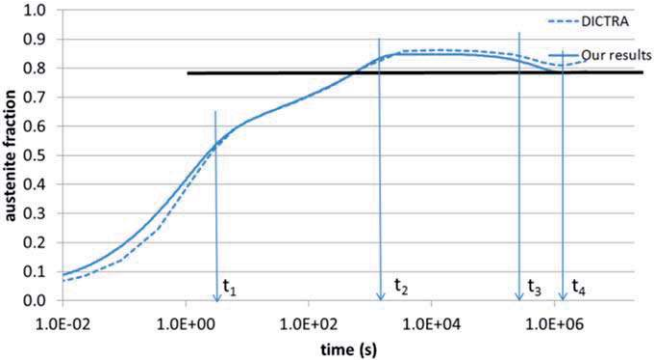

Figure 9. Modelled and DICTRA-simulated austenite formation kinetics during isothermal holding. The different reported times refer to different stages of austenite formation. Simulation conditions: $L = 5\ \mu$m, $T = 780\ ^{\circ}$C, $c_c^{\mathrm{Mn}} = 13$ wt%. The black line is the austenite fraction at ortho-equilibrium.

The agreement between the two solutions (figure 9) was very good, and the transformation kinetics appeared to be exactly the same. For short times ($t < 1$ s), the developed model slightly overestimates the austenite fraction. This overestimation originates from the assumption that cementite is instantaneously transformed into austenite. However, holding times of less than 1 s have limited industrial interest; therefore, these small differences may be ignored. The agreement between the two solutions is quite perfect for times ranging between 1 and 10 000 s, which is the range of industrial holding times for thermal treatments of such steel ($t < 300$ s). The first conclusion here is that it is not necessary to model cementite dissolution at 780 °C for an initial Mn concentration in cementite of 13 wt%.

For longer holding times, more differences are observed for the two solutions. The proposed model converges towards the ortho-equilibrium fraction given by the thermodynamic database of Thermo-Calc. The time to reach the steady state is longer for DICTRA, and the equilibrium is not the ortho-equilibrium because of the mass conservation issue. Once again, holding times longer than several hours are not of interest for material processing. However, long time evolution can be interesting when studying material ageing.

4.3. Mechanisms of austenite growth

The isothermal austenite formation kinetics in figure 9 are characteristic of austenite growth. Figures 10 and 11 present C and Mn concentration profiles at different times to clarify the diffusion mechanisms driving the phase change:

- For $t < t_1$: the austenite fraction rapidly increases owing to C diffusion, whereas Mn does not diffuse. The Mn concentration profile is only modified around the interface, resulting in a solute spike (figure 11) consistent with the condition of the equality of the interface velocity of each species (equation (5)) and the assumption of local thermodynamic equilibrium.
- For $t_1 < t < t_2$: the austenite fraction still increases and is controlled by Mn diffusion in ferrite. The C concentration in each phase is almost flat. However, the Mn concentration profile is significantly modified around the interface, leading to a higher flux of Mn from ferrite to austenite.

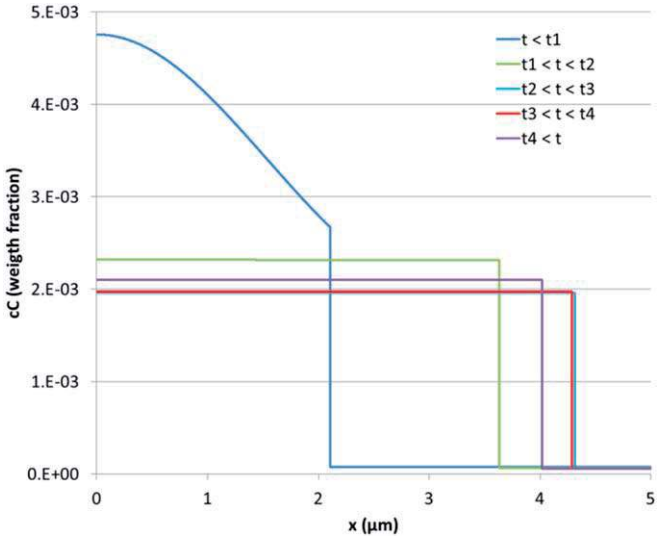

Figure 10. C concentration profiles at different simulation times reported in figure 9.

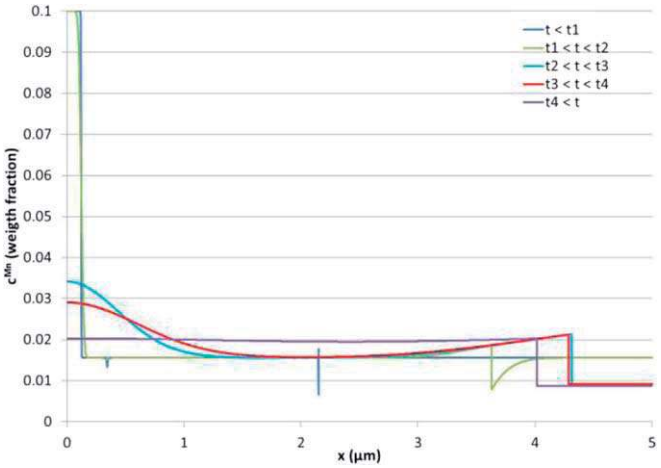

Figure 11. Mn concentration profiles at different simulation times reported in figure 9. The characteristic Mn spike of local equilibrium is observed for times shorter than $t < t_1$.

- For $t_2 < t < t_3$: the interface position is almost constant. The C concentration has been homogenized in austenite and ferrite. Mn from the original cementite slowly diffuses in austenite until it reaches the interface front.
- For $t_3 < t < t_4$: the austenite fraction decreases because of the homogenization of Mn in the austenite phase. Mn from the original cementite diffuses towards the austenite/ferrite interface and migrates into ferrite. This stage is the so-called austenite shrinkage stage.
- For $t > t_4$, equilibrium is reached. The concentration profiles are flat for austenite and ferrite. The system has reached the ortho-equilibrium.

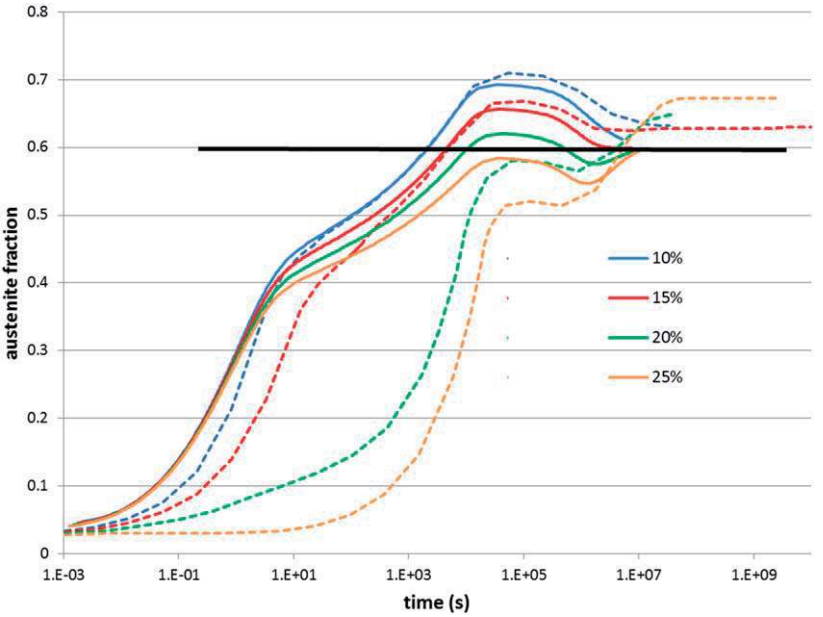

Figure 12. Modelled (full lines) and DICTRA-simulated (dashed lines) austenite formation kinetics during isothermal holding at 760 °C for Mn content in cementite of 10, 15, 20, and 25 wt% and $L = 6\ \mu$m.

4.4. Effect of cementite Mn concentration

For a system length $L = 6\ \mu$m and a holding temperature of 760 °C, the austenite formation kinetics were calculated using DICTRA and the developed model for initial Mn concentrations in cementite of 10, 15, 20, and 25 wt% (figure 12). The proposed model results in faster variations of the austenite fractions for the first stage than DICTRA. This difference is observed because DICTRA accounts for cementite dissolution, whereas our model assumes that cementite instantaneously transforms into austenite. The comparison reveals that the difference between the two models decreases when the Mn initial concentration in cementite is low enough; Mn in cementite slows down the cementite dissolution, as demonstrated in [41].

The austenite fraction at different stages depends on the initial Mn content in cementite. For high Mn content (larger than 20 wt%), the transformation kinetics is much faster with our model than with DICTRA. Two differences may explain this deviation: cementite dissolution and/or austenite nucleation, both modelled in DICTRA and not accounted for in our model.

4.5. Comparison with experimental results

The simulation results obtained using scenario one are compared with the experimental values in figure 13, which shows the austenite fraction evolution during isothermal treatment at 735 °C, 760 °C, and 780 °C. Note that for the experimental results, the austenite fraction is given as a function of the holding time (without accounting for the heating time).

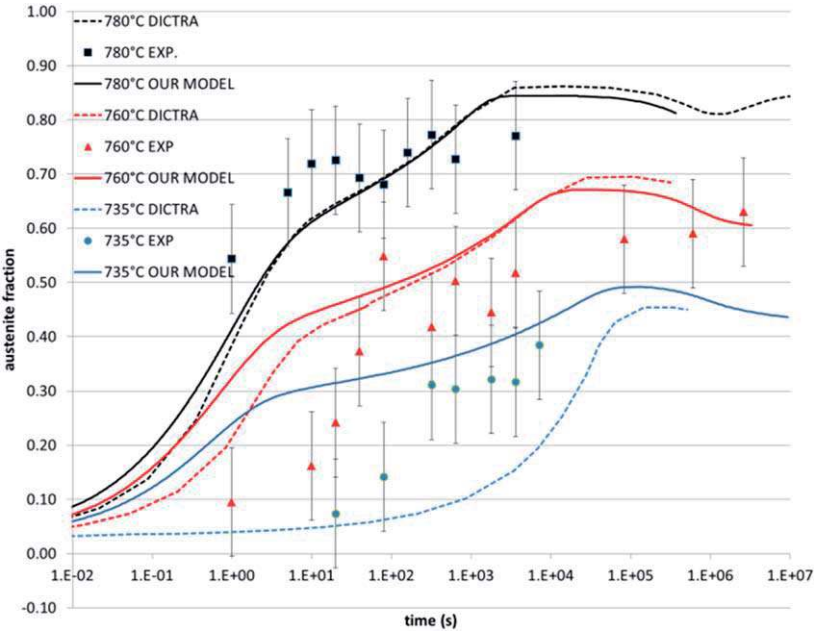

Figure 13. Experimental, modelled, and DICTRA-simulated austenite formation kinetics during isothermal holding at temperatures of 735 °C, 760 °C, and 780 °C. The so-called 'D' kinetics takes into account austenite nucleation when the driving force for precipitation exceeds 10^{-5} RT (J mol^{-1}). The Mn content of cementite was fixed at 13 wt% with a system size equal to $L = 5$ μm.

Consequently, as the experimental heating duration is approximately 7–8 s, comparison of the model and experiments for holding times shorter than 10 s is not relevant.

For the comparison with experimental data, to respect the periodicity of the system, the system length L considered for the model is $L_p/2 = 5$ μm (see figure 7). The initial Mn concentration in cementite was set to 13 wt%, corresponding to the measured value (see section 4.1). Experimentally, the absolute uncertainty on the austenite fraction is approximately 0.1.

For all temperatures and holding times larger than 100 s, the agreement between the developed model and experimental results is quite satisfactory in terms of both the transformation kinetics and austenite fraction levels. For the lower temperatures (760 °C and 735 °C), our model overestimates the transformation kinetics but gives the correct austenite fraction for holding times ranging from 100 to 10 000 s. This disagreement in the kinetics originates from the assumption of instantaneous cementite transformation into austenite made in our model (see section 2). As discussed by Gouné [41], at temperatures lower than 750 °C, the kinetics of cementite dissolution is drastically slowed down when the Mn concentration increases (from 6.7 wt% to 15.5 wt%). In our case, the Mn concentration is 13 wt%. Therefore, we may expect that this phenomenon is not negligible.

The strong deviation of the DICTRA-simulated kinetics (taking into account austenite nucleation) from the experimental kinetics is apparent at 735 °C. The nucleation module proposed in DICTRA may not be realistic (heterogeneous nucleation may strongly accelerate nucleation processes).

5. Conclusion

A 1D model for prediction of the ferrite-to-austenite transformation during intercritical thermal treatment of a ternary Fe–X–Y alloy is proposed. This model is based on the assumption that the solute element concentrations are at equilibrium at the ferrite/austenite interface (local equilibrium). An original numerical solution was developed to ensure exact mass conservation of the solute atoms; it predicts the concentration field of solutes and the interface position.

The model and its numerical solution were first validated using original data from the literature for steels with a 1D lamellar microstructure. Good agreement with the experimental data was observed for the isothermal transformation kinetics at various temperatures. Compared with previous models, the transformation kinetics showed fairly good agreement except for long treatment durations: our numerical solution tends towards the final ortho-equilibrium solution, as expected. This improvement is possible because the solution ensures the perfect mass conservation of the solutes. As the solution perfectly conserves the solute mass, it can be used to predict the large holding times that must be considered when studying material ageing.

The programme is fully open, enabling selection of the appropriate thermodynamic database and management of the numerical parameters to optimize the computational time.

The model was applied to a high-strength, low-alloyed Fe–C–Mn DP steel with a bi-layered structure; one layer was almost pure ferrite and the other was ferrite with cementite precipitates. The periodicity of the structure had a typical length of 10 μm. Assuming that cementite instantaneously transforms into austenite, the model showed that as long as short treatment durations ($<$10 s) are not of interest, regardless of the cementite distribution in the enriched layer, the transformation kinetics were the same. Thus, from the transformation kinetics viewpoint, the material can be modelled by a bilayer system composed of a layer of cementite and a layer of ferrite. Analysis of the C and Mn concentration profiles during the simulation confirmed that the austenite fraction in the system first depends on the C diffusion, then on the Mn redistribution in the system, and finally on the Mn homogenization in each phase.

To elucidate the effect of the cementite dissolution and austenite nucleation, our solution was compared with one obtained using DICTRA that accounts for cementite dissolution and austenite nucleation. It appears that cementite dissolution and austenite nucleation slow down the transformation kinetics. This trend is more important when the Mn initial concentration in cementite increases and the temperature decreases. Even if this phenomenon has already been demonstrated experimentally, these simulations allow this effect to be quantified.

With this comparison, it was also possible to determine that in DICTRA, the non-conservation of the solute masses only affects the kinetics transformation for long treatment durations.

The comparison between our model, DICTRA simulations, and experimental data was also interesting. As expected, the results of our model and the DICTRA simulations agreed well with the experimental values at high holding temperatures for which the cementite dissolution kinetics is faster than austenite growth. When the holding temperature was lower, our model showed good agreement for holding times larger than 100 s; however, the model overestimated the austenite fraction for holding times of less than 100 s. This finding is logical because cementite dissolution and austenite nucleation are not taken into account, and the austenite fraction kinetics is thus accelerated. Less expected was the underestimation of the austenite fraction when using DICTRA for the lowest holding temperature for the entire transformation kinetics. In that case, it might be important to account for the real geometry of the cementite: small precipitates instead of a thick layer would dissolve faster. However, this would require 1D simulation of a spherical precipitate; the whole system can then not be

simulated. Another parameter, the austenite nucleation driving force, might also be adapted but, it is not possible, with the actual model, to separate the influence of the cementite dissolution and austenite nucleation.

As a conclusion, the fair agreement between our model and experimental results for the low-alloyed Fe–C–Mn DP steel isothermal treatments, shows that for the whole temperature range of the isothermal treatments (735 °C–780 °C) and holding time that are interesting for industrial processes, it is not necessary to account for the cementite dissolution and austenite nucleation. This simplification is important since it leads to a simpler modelling and then reduced computational time.

Acknowledgments

Anthony Rollett is gratefully acknowledged for fruitful and stimulating discussions on the modelling of the DP steel.

ORCID iDs

P Chantrenne https://orcid.org/0000-0002-7036-2600
M Perez https://orcid.org/0000-0002-7350-4803

References

[1] Scott C, Allain S, Faral M and Guelton N 2006 The development of a new Fe–Mn–C austenitic steel for automotive applications *Rev. Met. Paris* **103** 293–302
[2] Lai Q, Gouné M, Perlade A, Pardoen T, Jacques P, Bouaziz O and Bréchet Y 2016 Mechanism of austenite formation from spheroidized microstructure in an intermediate Fe–0.1C–3.5Mn steel *Metall. Mater. Trans.* A **47** 3375–86
[3] Speich G R, Demarest V A and Miller R L 1981 Formation of austenite during intercritical annealing of dual-phase steels *Metall. Mater. Trans.* A **12** 1419–28
[4] Barbier D, Germain L, Hazotte A, Gouné M and Chbihi A 2015 Microstructures resulting from the interaction between ferrite recrystallization and austenite formation in dual-phase steels *J. Mater. Sci.* **50** 374–81
[5] Chbihi A, Barbier D, Germain L, Hazotte A and Gouné M 2014 Interactions between ferrite recrystallization and austenite formation in high-strength steels *J. Mater. Sci.* **49** 3608–21
[6] Ollat M, Massardier V, Fabregue D, Buscarlet E, Keovilay F and Perez M 2017 Modeling of the recrystallization and austenite formation overlapping in cold-rolled dual-phase steels during intercritical treatments *Metall. Mater. Trans.* A **48** 4486–99
[7] Murray W D and Landis F 1959 Numerical and machine solutions of transient heat-conduction problems involving melting or freezing: part I—method of analysis and sample solutions *J. Heat Transfer* **81** 106–12
[8] Sarler B 1995 Stefan's work on solid-liquid phase changes *Eng. Anal. Bound. Elem.* **16** 83–92
[9] Illingworth T C and Golosnoy I O 2005 Numerical solutions of diffusion-controlled moving boundary problems which conserve solute *J. Comput. Phys.* **209** 207–25
[10] Gouné M, Danoix F, Ågren J, Bréchet Y, Hutchinson C R, Militzer M, Purdy G, van der Zwaag S and Zurob H 2015 Overview of the current issues in austenite to ferrite transformation and the role of migrating interfaces therein for low alloyed steels *Mater. Sci. Eng.* R **92** 1–38
[11] Avrami M 1939 Kinetics of phase change: I. General theory *J. Chem. Phys.* **7** 1103–12
[12] Kulakov M, Poole W J and Militzer M 2014 A microstructure evolution model for intercritical annealing of a low-carbon dual-phase steel *ISIJ Int.* **54** 2627–36
[13] Crespo D and Pradell T 1996 Evaluation of time-dependent grain-size populations for nucleation and growth kinetics *Phys. Rev.* B **54** 3101–9

[14] Crespo D, Pradell T, Clavaguera-Mora M T and Clavaguera N 1997 Microstructural evaluation of primary crystallization with diffusion-controlled grain growth *Phys. Rev.* B **55** 3435–44
[15] Christian J W 1981 *The Theory of Transformations in Metals and Alloys* (Oxford: Pergamon)
[16] Ollat M, Militzer M, Massardier V, Fabregue D, Buscarlet E, Keovilay F and Perez M 2018 Mixed-mode model for ferrite-to-austenite phase transformation in dual-phase steel *Comput. Mater. Sci.* **149** 282–90
[17] Sietsma J and van der Zwaag S 2004 A concise model for mixed-mode phase transformations in the solid state *Acta Mater.* **52** 4143–52
[18] Chen H and van der Zwaag S 2014 Predicting the effect of Mo, Ni, and Si on the bainitic stasis *Metall. Mater. Trans.* A **45** 3429–37
[19] Purdy G R and Brechet Y J M 1995 A solute drag treatment of the effects of alloying elements on the rate of the proeutectoid ferrite transformation in steels *Acta Metall. Mater.* **43** 3763–74
[20] Steinbach I 2009 Phase-field models in materials science *Modelling Simul. Mater. Sci. Eng.* **17** 073001
[21] Gurtin M E 1996 Generalized Ginzburg–Landau and Cahn-Hilliard equations based on a microforce balance *Physica* D **92** 178–92
[22] Huang C, Browne D and Mcfadden S 2006 A phase-field simulation of austenite to ferrite transformation kinetics in low carbon steels *Acta Mater.* **54** 11–21
[23] Mecozzi M G, Sietsma J and van der Zwaag S 2006 Analysis of $\gamma \rightarrow \alpha$ transformation in a Nb micro-alloyed C–Mn steel by phase field modelling *Acta Mater.* **54** 1431–40
[24] Pariser G, Schaffnit P, Steinbach I and Bleck W 2001 Simulation of the γ–α-transformation using the phase-field method *Steel Res.* **72** 354–60
[25] Mecozzi M G, Bos C and Sietsma J 2015 A mixed-mode model for the ferrite-to-austenite transformation in a ferrite/pearlite microstructure *Acta Mater.* **88** 302–13
[26] Zhu B and Militzer M 2015 Phase-field modeling for intercritical annealing of a dual-phase steel *Metall. Mater. Trans.* A **46** 1073–84
[27] Wycliffe P A, Purdy G R and Embury J D 1981 Growth of Austenite in the intercritical annealing of Fe–C–Mn dual phase steels *Can. Metall. Q.* **20** 339–50
[28] Andersson J-O, Helander T, Höglund L, Shi P and Sundman B 2002 Thermo-Calc & DICTRA, computational tools for materials science *Calphad* **26** 273–312
[29] Saied M 2016 *Experimental and Numerical Modeling of the Dissolution of Delta Ferrite in the Fe–Cr–Ni System: Application to the Austenitic Stainless Steels* Université Grenoble Alpes Thesis
[30] Vitek J M, Vitek S A and David S A 1995 Numerical modeling of diffusion-controlled phase transformations in ternary systems and application to the ferrite/austenite transformation in the Fe–Cr–Ni system *Metall. Mater. Trans.* A **26A** 2007–25
[31] Kajihara M, Lim C B and Kikuchi M 1993 Experimental study on dissolution of alpha phase in gamma/alpha/gamma diffusion couples of the Fe–Cr–Ni system *ISIJ Int.* **33** 498–507
[32] Larsson H 2014 A model for 1D multiphase moving phase boundary simulations under local equilibrium conditions *Calphad* **47** 1–8
[33] Kajihara M and Kikuchi M 1993 Numerical analysis of dissolution of alpha phase in gamma/alpha/gamma diffusion couples of the Fe–Cr–Ni system *Acta Metall. Mater.* **41** 2045–59
[34] Nougier J P 1987 *Méthode de Calcul Numérique* (Paris: Masson)
[35] Shih T M 1982 *Numerical Heat Transfer* (Washington: Hemisphere Publishing Coorporation)
[36] Wylie C R and Barret L C 1985 *Advanced Engineering Mathematics* (Singapore: Mc Graw Hill Book Company)
[37] Rothman S J, Nowicki L J and Murch G E 1980 Self-diffusion in austenitic Fe–Cr–Ni alloys *J. Phys. F: Met. Phys.* **10** 383–98
[38] Kirchner G, Nishizawa T and Uhrenius B 1972 The distribution of chromium between ferrite and austenite and the thermodynamics of the out of equilibrium in the Fe–Cr and Fe–Mn systems *Metall. Trans.* **4** 167–74
[39] Savran V I, Van Leeuwen Y, Hanlon D N, Kwakernaak C, Sloof W G and Sietsma J 2007 Microstructural features of austenite formation in C35 and C45 alloys *Metall. Mater. Trans.* A **38** 946–55
[40] Ollat M 2017 *Characterization and Modeling of Microstructural Evolutions During the Thermal Treatment of Cold-Rolled Dual-Phase Steels* Université de Lyon Thesis
[41] Gouné M, Maugis P and Drillet J 2012 A criterion for the change from fast to slow regime of cementite dissolution in Fe–C–Mn steels *J. Mater. Sci. Technol.* **28** 728–36